Romanian Reports in Physics, Vol. 66, No. 3, P. 778–787, 2014

USING AFM TOPOGRAPHY MEASUREMENTS IN NANOPARTICLE SIZING

D. CHICEA[1,2]

[1] "Lucian Blaga" University of Sibiu, Environmental Sciences Department, Dr. Ion Ratiu Str. 7-9, Sibiu, 550012, Romania, dan.chicea@ulbsibiu.ro
[2] Pediatric Respiratory Medicine Research Center (CCMRP), Str. Pompeiu Onofreiu Nr. 2– 4, Sibiu

Received July 19, 2013

Abstract. Two simple recipes for preparing Fe_3O_4 nanoparticles are briefly presented. The nanoparticles were characterized using Dynamic Light Scattering and Atomic Force Microscopy. The results of the DLS procedure are presented in detail and discussed in connection with the AFM results, highlighting the differences between the size distribution in connection with the preparation parameters.

Key words: dynamic light scattering, atomic force microscopy, Fe_3O_4 nanoparticles.

1. INTRODUCTION

Nanoparticle structured materials have been used to investigate living cells or to deliver certain substances or drugs to them. This is possible as the nanoparticle dimension is smaller than the cell organelles. Certain applications of nanostructured materials in biology and medicine have been developed and are presented in review papers, [1] being just one of them. In recent years warnings on the potential danger of the nanoparticles in environment were issued [2] though. Consequently different techniques of detection and monitoring the nanoparticle concentration are presented in the literature [2].

Nanoparticle penetration through the cell membrane strongly depends of the nanoparticles physico-chemical properties as shape, size, surface charge, surface chemistry [3], therefore it is of interest to characterize the nanoparticles size and size distribution prior of using them in biomedical applications.

Fe_3O_4 nanoparticles are of special interest for biomedical applications because they are not toxic [4] and they can be metabolized by living organisms [4]. They present a major inconvenient though, as they aggregate very fast in diluted aqueous suspension [5], as the body fluids are. The former nanofluid quickly exhibits micron sized particles in suspension.

Transmission Electron Microscopy (TEM), Ferromagnetic resonance (FMR), and X-ray powder diffraction, are some of the techniques that are widely used in nanoparticle size characterization. Optical techniques appear to be convenient for nanoparticle size characterization [6]. If a suspension is the target of a coherent light beam, the image changes in time and presents fluctuations as a consequence of the scattering centers complex motion of both sedimentation and Brownian motion [7, 8]. Dynamic Light Scattering (DLS) or Photon Correlation Spectroscopy (PCS) is the optical method that uses the correlation of the speckle dynamics with the Brownian motion [7, 8, 9].

A simple coprecipitation method with different values of the physical synthesis parameters was used in the work described here for preparing two nanofluid samples. The DLS was used as a standard method to characterize the nanoparticles size. In addition the AFM technique was used as an alternative method to characterize the nanoparticle size. Typically an AFM scan is carried on and surface topography images are presented together with a rough range of the grain size [10]. In this article the grain statistics [11] was used to assess the nanoparticle size distribution.

The differences in the results of the nanoparticles size characterization using the two methods are presented and the results suggest that the AFM technique can be used as a standard method for nanoparticle size characterization.

As the size of the nanoparticles is crucial for nanoparticles biomedical application, the two methods were used to investigate the effects of the temperature and stirring intensity on the nanoparticles size distribution and the results are presented, as well.

2. MATERIALS AND METHOD

2.1. NANOFLUID PREPARATION

The procedure that was used to prepare the first aqueous nanofluid sample (hereafter sample A) was a typical coprecipitation. The reagents used were: $FeCl_2 \cdot 4H_2O$, $FeCl_3 \cdot 6H_2O$, ammonium hydroxide (NH_3[aq]), citric acid ($C_6H_8O_7$), produced by Merck. Double deionised water was used to dissolve the reagents.

Overall the chemical reaction was:

$$2FeCl_3 + FeCl_2 + 8NH_3 + 4H_2O \rightarrow Fe_3O_4 + 8NH_4Cl. \quad (1)$$

The synthesis temperature considerably changes the size distribution and the chemical composition [12, 13] of the nanoparticles. Reference [14] states that using a temperature range of 65–75^{0}C will produce spherical magnetite nanoparticles. The nanofluid synthesis procedure resembles very much the procedure presented in [15], which contains a detailed description, but it is apart from it in one aspect. The

coprecipitation stage of the synthesis procedure, when the ammonium hydroxide was added drop by drop, was carried on at 72°C and not at 80°C as in [15]; a strong stirring was maintained during the entire stage, as in [15].

The volume fraction φ of nanoparticle phase in the nanofluid sample was calculated from mass density measurements using Eq. 2:

$$\varphi = \frac{\rho_f - \rho_l}{\rho_s - \rho_l}, \tag{2}$$

where ρ_f is the ferrofluid density, ρ_l the density of the carrier fluid and ρ_s the density of the solid particles. Using Eq. 2 we found that the volume fraction φ of nanoparticles was 15.7%.

The procedure was repeated in order to produce the sample B, but with modified values of the physical parameters. The coprecipitation stage of the synthesis procedure was carried on at room temperature, which was 22°C and stirring was week, yet constant. The procedure resembles much more the recipe that was used in [16] than the procedure used to produce sample A. The nanoparticles of the two samples were analyzed first using the DLS technique which is briefly presented in the next subsection.

2.2. DYNAMIC LIGHT SCATTERING NANOPARTICLE CHARACTERIZATION

The experimental works [17, 18] proved that the power spectrum of the scattered light intensity can be linked to the probability density function (hereafter PDF). According to the Wiener-Khintchine-Theorem, this translation of the scattering particles motion into phase differences relates the power spectrum to the autocorrelation function of a process. A typical DLS experimental setup is presented in Fig. 1 and consists of a laser, a detector, a data acquisition system and a computer.

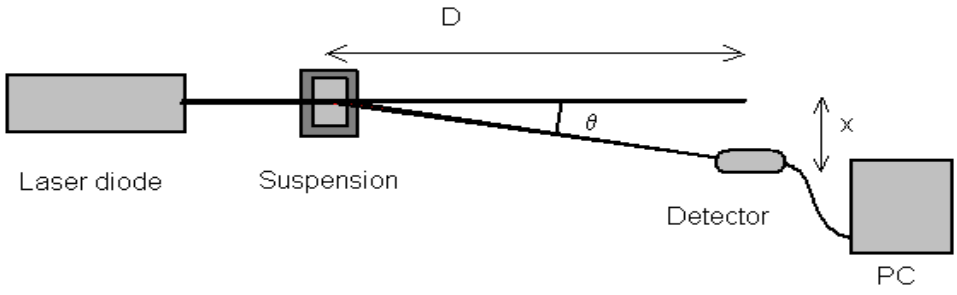

Fig. 1 – The DLS experimental setup, view from above.

The power time series is obtained by subtracting the average intensity from the recorded time series and by squaring the output. The Fourier transform of the power time series is the power spectrum. The spectrum calculated from the experimental data can be compared with the theoretically expected spectrum, which is the functional form of the Lorentzian line *S(f)* in Eq. 3. The Lorentzian *S(f)* has two free parameters a_0 and a_1, which can be found using a least square minimization procedure:

$$S(f) = a_0 \cdot \frac{a_1}{(2\pi f)^2 + a_1^2}. \tag{3}$$

The diameter of the scattering centers can be assessed as the double of the radius *R* using Eq. 4.

$$R = \frac{2k_B TK^2}{6\pi\eta a_1}, \quad \text{where} \quad K = \frac{4\pi n}{\lambda} \cdot \sin\frac{\theta}{2}. \tag{4}$$

In (4) *T* is the absolute temperature of the sample, k_B is Boltzman's constant, η is the dynamic viscosity of the solvent, θ is the scattering angle, *n* is the refractive index of the scattering particles and λ is the wavelength of the laser radiation in vacuum.

The light source was a laser diode operating continuously and the power was 21 mW. The wavelength of the laser beam was 635 nm. The DLS experiment was conducted at 20°C. The cuvette-detector distance D = 0.46 m and x = 0.040 m, thus the scattering angle θ was equal to 4° 58' 11''. These parameters are untypical; currently a scattering angle of 90° is used. The reason for using a smaller angle is to shift the rollover point, hence the a_1 parameter towards smaller frequencies, where the noise of the environment and data acquisition system is smaller. More details on the data processing procedure are presented in [6].

In order to avoid aggregation the concentrated nanoparticle suspension was diluted in 25% citric acid following the procedure described in [6] and a time series was recorded for each of the two samples and processed, as well.

2.3. AFM NANOPARTICLE CHARACTERIZATION

The AFM is a scanning probe microscope and uses a flexible cantilever to describe a profile while maintaining the force or electric current between the tip and sample constant [19]. By scanning the sample line by line and using a calibration file for each scanner a topography image of the surface is reconstructed and can be used in particle imaging and sizing [20].

The AFM that was used is an Agilent 5500. The scanning was carried on in tapping mode using the MAC scanner. A very soft tip, with the spring constant equal to 5 N/m was used at low force amplitude.

Sample preparation is crucial. The samples must be thin enough to have a single layer of the objects under investigation. Moreover, the objects to be imaged must stick well to the substrate and remain in the same position during scanning, otherwise they will be moved by the tip of the cantilever, producing artifacts and unrealistic images [20]. More details on the scanning using the AGILENT 5500 AFM, on systematic errors and on avoiding artifacts are presented in [5] and [21]. The samples were prepared using a procedure similar with the procedure reported in [5]. A small drop of the nanofluid was deposited on a freshly cleaved mica substrate, in order to have an un-contaminated substrate with atomic grade plane. It was stretched on the substrate using a sharp edge and allowed to evaporate for 5 hours at 22 ^{o}C in air and this procedure was followed for both samples A and B prior of scanning them.

Once the samples were scanned, the recordings were analyzed with the Gwyddion 2.25 (a free software developed under the GNU project of MIT, Cambridge, MA, USA) and the nanoparticle size distribution was assessed using the grain statistics feature [11].

3. RESULTS

3.1. DLS CHARACTERIZATION RESULTS

A time series was recorded for both samples A and B and were processed following the procedure described in 2.2. Figures 2 and 3 present the power spectrum density and the fitted Lorentzian line for samples A and B.

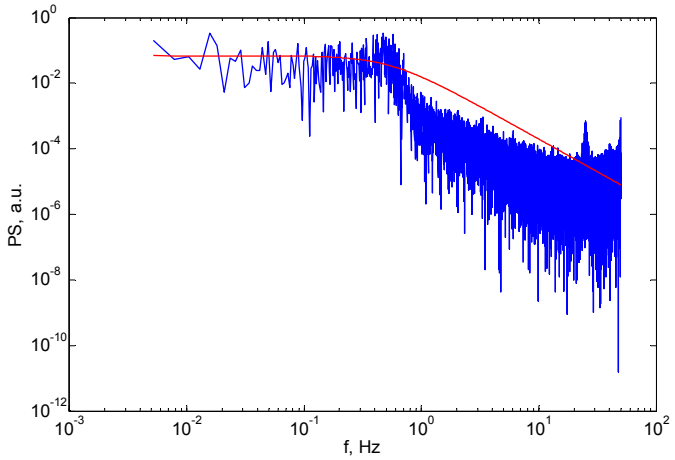

Fig. 2 – The PSD (scattered line) and the fitted Lorentzian line (smooth line) for time series slice recorded for nanofluid A.

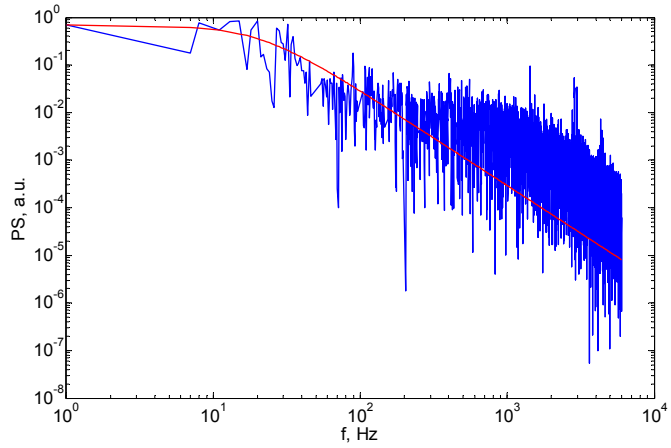

Fig. 3 – The PSD (scattered line) and the fitted Lorentzian line (smooth line) for time series slice recorded for nanofluid B.

After fitting the curve described by Eq. (3) and after using Eq. (4) the average diameter of the nanoparticles was found to be 21 nm for the nanoparticles suspended in nanofluid A and 410 nm for nanofluid B.

3.2. AFM CHARACTERIZATION RESULTS

A good resolution scan (512 × 512) was achieved for a surface of 0.5 μm × 0.5 μm for sample A, as it has smaller nanoparticles and of 50 μm × 50 μm for sample B, which has bigger nanoparticles, following the procedure described in [20]. Data acquisition was followed by image processing procedure, the same for both samples. First a three point leveling was applied, to correct the possible and frequently appearing small tilt of the substrate. The horizontal artifact lines were removed followed by the "scar removal" procedure. A 3D rendering type of the surface topography of sample A is presented in Fig. 4 and of sample B in Fig. 5.

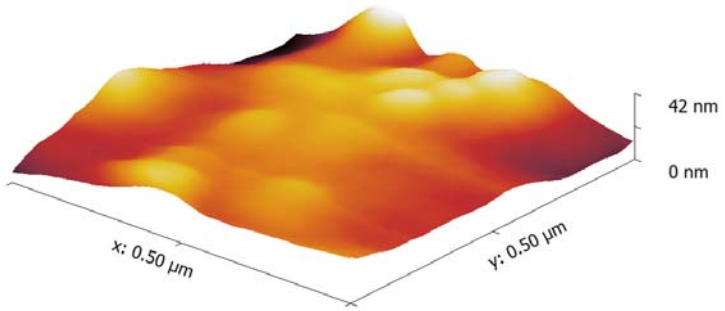

Fig. 4 – A 3D surface topography image of sample A.

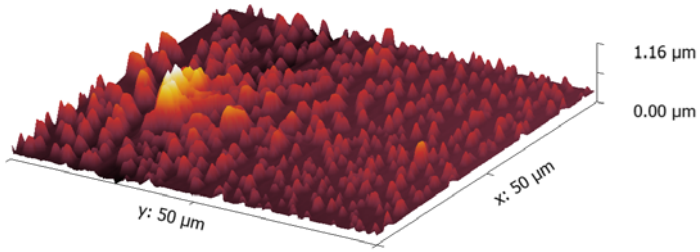

Fig. 5 – A 3D surface topography image of sample B.

The acquired data was processed further on by performing a grain statistics, using Gwyddion 2.25. The grains were marked using the Laplaceian algorithm with the same threshold of 44%. The grain distribution was computed with the same Gwyddion 2.25 by selecting the mean value of the grain size as an output. The plot of the grain size distribution for the surface topography of sample A (Fig. 4) is presented in Fig. 6 and for the surface topography of sample B (Fig. 5) is presented in Fig. 7.

Examining Figs. 6 and 7 we notice that the maximum of the grain size distribution is located at 20 nm for sample A and at 346 nm for sample B. We also notice that the grain size distribution is not quite a perfect Gaussian line, as in [20] and this can be explained by the smaller number of objects that were present on the surface and were therefore subject of the statistical analysis. The size of the surface that was scanned for the two samples is a compromise between describing a smaller number of particles (hence a poor statistics) but with a good resolution (512×512 pixels) for each nanoparticle and having a bigger number of particles (hence a better statistics), each nanoparticle being described using a smaller number of pixels though. Considering the result of the DLS analysis the 0.5 µm × 0.5 µm for sample A, and of 50 µm × 50 µm for sample B is the result of the optimization process presented above.

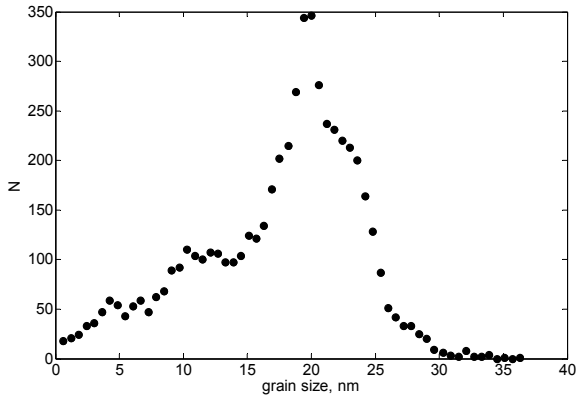

Fig. 6 – The nanoparticle size distribution for sample A.

The value of the maximum of the grain size distribution is different from the average grain size. A weigh average of the grain size, hence nanoparticle size, was computed for the two samples using the data with the grain size distributions presented in Figs. 6 and 7. The average nanoparticle size was found to be 17.4 nm for sample A and 367 nm for sample B.

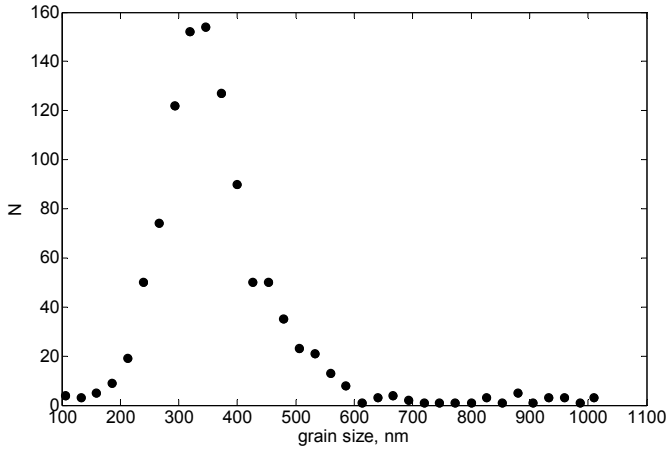

Fig. 7 – The nanoparticle size distribution for sample B.

The results of the DLS and AFM analyses are presented in Table 1.

Table 1

The average nanparticles diameter of the two samples A and B assessed by DLS and AFM

Sample	A	B
DLS average diameter, nm	21	410
AFM average diameter, nm	17.4	367

4. CONCLUSION AND DISCUSSIONS

Two nanofluids having Fe_3O_4 nanoparticles in suspension were synthesized following a coprecipitaion procedure, but using different temperatures during the coprecipitation stage, 72 ^oC for nanofluid A and 22 ^oC for nanofluid B. Stirring was intense during the coprecipitation stage for nanofluid A and week for nanofluid B.

The nanoparticle size analysis was carried on using the DLS technique as reference and the AFM technique. The DLS average nanoparticle size was found to be 21 nm for nanofluid A and 410 nm for nanofluid B. AFM was used to characterize the samples, as well. We found that the average nanoparticle diameter was 17.4 nm for sample A and 367 nm for sample B. These differences, of –17%

for sample A and –10% for sample B can be the result of the systematic errors between the methods. The DLS technique has, as an output, the hydrodynamic diameter, which is slightly bigger than the physical diameter [6]. The AFM diameter is the result of measuring a grain of tens of nanometers with a tip having the radius around 50 nm [21]. These results, exhibiting an DLS measured diameter bigger than the AFM measured diameter, are consistent with the results reported in [22], which reveal that the AFM measured nanoparticle diameter appears to be reduced with 20%. These differences between the results on size assessment are not surprising. Big differences between methods that use different physical procedures are reported in many papers, [22] and [23] being just two of them.

Nevertheless, the results presented in this work reveal that the AFM technique, although slow compared with the DLS, can provide useful information regarding the size distribution of the nanoparticles. Moreover, the results reveal that the size distribution can be controlled during the simple coprecipitation synthesis method, by adjusting the temperature and the stirring intensity. A relatively big temperature, around 75^{o}C combined with a strong stirring leads to smaller nanoparticles while a lower temperature and weak stirring leads to bigger sized nanoparticles, and this can be useful in manufacturing nanoparticles for biomedical applications. Similar work on temperature influence on nanoparticle size distribution, for gold nanoparticles though, is reported in [24], which explains the influence of the temperature by the frequency of the collisions of gold ions. Reference [25] reports on manufacturing Fe_3O_4 nanoparticles as well, but using a different recipe though, and in a totally different temperature range, which is 250-290^{o}C. The results in [25] are contrary with the results reported here and the explanation lays primarily in the synthesis procedure.

REFERENCES

1. O.V. Salata, Journal of Nanobiotechnology, **2**, *3* (2004); doi:10.1186/1477-3155-2-3.
2. G.G. Leppard, Current Nanoscience **4**, *2*, 278–301 (2008).
3. L. Treuel, X.E. Jiang, G.U. Nienhaus, Journal of The Royal Society Interface, **10**, *82*, 20120939 (2013); doi: 10.1098/rsif.2012.0939.
4. W.K. Tseng, J.J. Chieh, Y.F. Yang, C.K. Chiang, Y.L. Che et al., PLoS ONE, **7**, *11*, e48510, 2012; doi:10.1371/journal.pone.0048510.
5. D. Chicea, Optoelectronics and Advanced Materials – Rapid Communications, **4**, *9*, 1310–1315 (2010).
6. D. Chicea, Current Nanoscience, **8**, *2*, 259–265 (2012).
7. J.W. Goodman, *Laser speckle and related phenomena*, Vol. 9 *Topics in Applied Physics*, J.C. Dainty (Ed.), Springer-Verlag, Berlin, Heidelberg, New York, Tokyo, 1984.
8. Briers J. D. Laser Doppler, Physiol. Meas., **22**, R35–R66 (2001).
9. M. Giglio, M. Carpineti, A. Vailati and D. Brogioli, Appl. Opt., **40**, *24*, 4036–4040 (2001).
10. A. Rao, M. Schoenenberger, E. Gnecco, Th. Glatzel, E. Meyer, J. Phys.: Conf. Ser., **61**, 971–976 (2006); doi:10.1088/1742-6596/61/1/192

11. Petr Klapetek, Ivan Ohlídal, Daniel Franta, Alberto Montaigne-Ramil, Alberta Bonanni, David Stifter, Helmut Sitter, Acta Physica Slovaca, **3**, 223–230 (2003).
12. Z.L Liu, Y.J. Liu, K.L. Yao, Y.H. Ding, J. Tao, X. Wang, Journal of Materials Synthesis and Processing, **10**, 83–87 (2002).
13. L.Vayssieres, C. Chaneac, E. Tronc, J.P. Jolinet, Journal of Colloid and Interface Science, **205**, 205–212 (1998).
14. G.F. Goya, T.S. Berquo, F.C. Fonseca, M.P., Morales, Journal of Applied Physics, **94**, 3520–3528 (2003).
15. D. Chicea, E. Indrea, C. M. Cretu, Journal of Optoelectronics and Advanced Materials, **14**, *5–6*, 46–466 (2012).
16. 7. D. Chicea, C. M. Goncea, Optoelectronics and Advanced Materials – Rapid Communications, **3**, *3*, 185–189 (2009).
17. N.A. Clark, J.H. Lunacek, G.B. Benedek, American Journal of Physics, **38**, *5*, 575–585 (1970).
18. S.B. Dubin, J.H. Lunacek, G.B. Benedek: PNAS, **57**, *5*, 1164–1171 (1967).
19. *** http://www.jpk.com/general-scanning-probe-microscopy.431.html
20. D. Chicea, R. Chicea, L. M. Chicea, Romanian Reports in Physics, **65**, *1*, 178–185 (2013).
21. D. Chicea, B. Neamtu, R. Chicea, L. M. Chicea, Digest Journal of Nanomaterials and Biostructures, **5**, *3*, 1033–1040 (2010).
22. F. Zhang, S.W. Chan, J. E. Spanier, E. Apak, Q. Jin, R. D. Robinson, I. P. Herman, Appl. Phys. Lett., **80**, 27 (2002); doi:10.1063/1.1430502.
23. Y.F. Shena, J. Tanga, Z.H. Niea, Y.D.Wanga, Y. Renc, L. Zuoa, Separation and Purification Technology, **68**, 312–319 (2009).
24. Y. Hatakeyama, S. Takahashi, K. Nishikawa, J. Phys. Chem. C, **114**, *25*, 11098–11102 (2010); doi: 10.1021/jp102763n.
25. J. Xie, S. Peng, N. Brower, N. Pourmand, S. X.Wang, and S. Sun, Pure Appl. Chem., **78**, *5*, 1003–1014 (2006); doi:10.1351/pac200678051003.